THE JOURNAL OF PHYSICAL CHEMISTRY C

Article

pubs.acs.org/JPCC

Porous Aromatic Frameworks Impregnated with Lithiated Fullerenes for Natural Gas Purification

Afsana Ahmed,[†,‡] Ravichandar Babarao,[‡] Runhong Huang,[§] Nikhil Medhekar,[§] B. D. Todd,[†] Matthew R. Hill,[‡] and Aaron W. Thornton*[,‡]

[†]Department of Mathematics, School of Science, Faculty of Science, Engineering and Technology and Centre for Molecular Simulation, Swinburne University of Technology, Melbourne, VIC 3122, Australia

[‡]CSIRO Manufacturing Flagship, Private Bag 10, Clayton South MDC, VIC 3169, Australia

[§]Department of Materials Engineering, Monash University, Clayton, VIC 3168, Australia

Supporting Information

ABSTRACT: Natural gas, a lower emission alternative than its fossil fuel counterparts, requires the removal of carbon dioxide, known as "sweetening", prior to its use. In this study we computationally explore the separation of methane and carbon dioxide using a new adsorbent consisting of lithium-decorated fullerenes (Li_6C_{60}) impregnated within a series of porous aromatic frameworks (PAFs) of various pore sizes. The strong affinity of CO_2 with the impregnated frameworks, confirmed by density functional theory, leads to selective adsorption over CH_4. The impregnation can also double the CO_2 adsorption capacity compared to the bare PAF and increase selectivity of CO_2/CH_4 up to 48 for an optimum amount of Li_6C_{60}, which is above the current industry benchmark. Overall, the study reveals physical insights and proposes impregnated PAFs to be promising candidates for CO_2/CH_4 separations for natural gas purification.

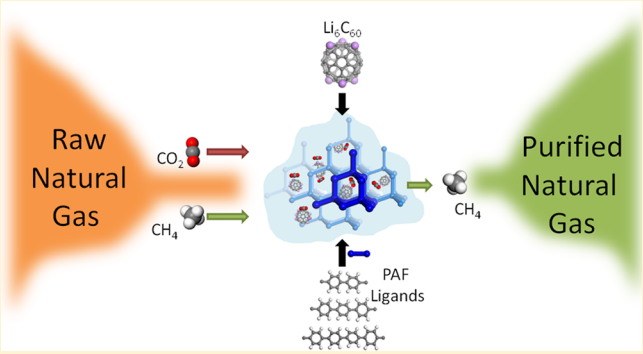

I. INTRODUCTION

Natural gas as a vehicular fuel has a number of advantages both economically and environmentally. Compared to other fossil fuels like gasoline or diesel, natural gas reduces the amount of byproduct of CO, CO_2, and SO_2 by 97, 24, and 90%, respectively.[1,2] Natural gas contains a variable amount of methane (CH_4) ranging from (27−95%), with a wide range of other components including CO_2 depending on the source;[3] see the world reservoir Table S1 (Supporting Information). The presence of CO_2 reduces the energy content of natural gas, contributes to climate change and often leads to pipeline corrosion.[1,4] To prevent this and also to increase the commercial value of natural gas, it should meet established purity specifications that are known as "pipeline-quality-methane". To meet this criteria, the maximum amount of CO_2 concentration cannot exceed 2%.[1] In addition, when natural gas is transported over great distances, the use of pipelines is too expensive and inefficient, and therefore liquefied natural gas (LNG) is a more efficient form of transport.[5] To make LNG, the gas is cooled to cryogenic conditions. During this process, the CO_2 present can freeze and block pipeline systems which will cause transportation issues.[6] In locations such as Germany (Central European Pannonian basin) or South Australia (Cooper Eromanga basin)[7] this CO_2 contamination exceeds 10%. As a result, it is critical to remove CO_2 from natural gas for economic, operational, safety, and environmental reasons.[8,9]

For the separation of CO_2 from a CO_2/CH_4 mixture, various technologies are available, such as chemical absorption,[10,11] thermal and pressure swing adsorption,[12,13] cryogenic distillation,[10] and membrane separation.[14,15] Among these gas separation techniques, adsorption-based separation has become a major gas separation tool in industry due to its inherent simplicity, ease of control, and relatively low operating costs.[3,16] However, with the growing global demand for natural gas, separations must become more efficient for natural gas to remain economically competitive above other harmful fuel alternatives.

Several families of microporous materials have been considered for the selective adsorption of CO_2/CH_4 mixtures such as zeolites, metal−organic frameworks, activated carbons, silica, nanotubes, and other inorganic structures.[4,9,17−21] In industry, for example, the adsorption process has been successfully implemented across the USA for the recovery of CH_4 from landfill gases using zeolites.[3,22] To further improve the performance of these systems, adsorbents must adsorb

Received: February 4, 2015
Revised: April 1, 2015
Published: April 2, 2015

DOI: 10.1021/acs.jpcc.5b01144
J. Phys. Chem. C 2015, 119, 9347−9354

more gas at higher selectivities while retaining chemical, physical, and thermal stability.

Porous aromatic frameworks (PAFs) were reported as a new family of ultraporous materials with surface areas above 5000 m^2/g, 5 times above that for zeolites, and thus capable of adsorbing copious amounts of gas. To date, most studies of adsorption in PAFs have focused on gas storage applications, and it is known that capacities can be drastically enhanced when the PAF surface is chemically functionalized.[23−26] We recently considered PAFs for enhancing volumetric hydrogen storage at low pressure.[27] Our work showed that the incorporation of lithiated fullerenes (Li_6C_{60}) in PAFs can enhance the volumetric capacity of H_2 from 12 to 44 g/L. Peng et al.[28] have used C_{60} intercalated graphite for purification of CO_2 from CH_4 and calculated a selectivity of 8. We expect that the metal sites on Li_6C_{60} will increase the polarization of CO_2 molecules and consquently achieve a higher CO_2/CH_4 selectivity than bare C_{60}.

Here we considered PAFs impregnated with Li_6C_{60} by enhancing volumetric surface area and tuning the porosity for the separation of CO_2 over CH_4, shown schematically in Figure 1. In this work, single component adsorption of CH_4 and CO_2 within Li_6C_{60} impregnated PAFs of various pore sizes at close to ambient conditions has been simulated. From the single component isotherms, the adsorption behavior of binary mixtures using the ideal adsorbed solution theory (IAST) was obtained.[29,30] Although this material may not be economically feasible, the scientific principles underlying the performance enhancement is of value. Structure−property relationships revealed the dominant structural characteristics responsible for enhanced separation. Finally, performances were benchmarked with conventional adsorbents.

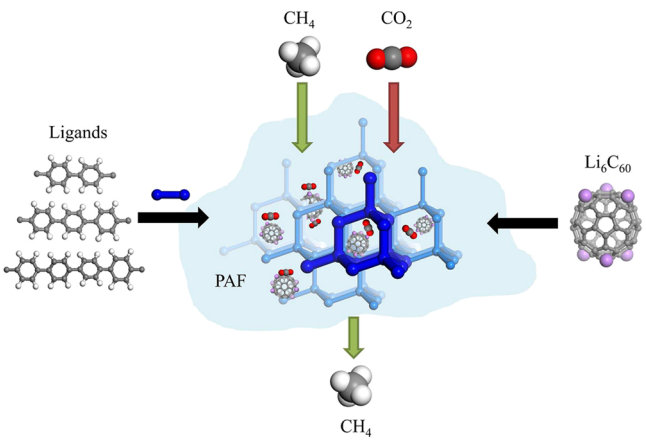

Figure 1. Schematic of CO_2/CH_4 separation in Li_6C_{60} impregnated PAF.

II. MODELS AND SIMULATION

In this work the PAF structures were constructed following details outlined by Lan et al.[31] The structures include PAF-30X (X = 1−4), where 3 means 3D structure and X denotes the number of phenyl rings used to replace the C−C bond. Each unit cell was constructed using the Forcite module of the Material Studio package with cubic periodic boundaries.[32] Lithiated fullerenes were randomly inserted within the PAF unit cell followed by geometry optimization.

Charges were assigned to each atom within the nLi_6C_{60}@PAF structures using density functional theory (DFT); see Figure S1 in the Supporting Information. We followed the calculation details of Babarao et al.[33] DFT was implemented in DMol3 on the basis of fragmental clusters.[34] The cleaved bonds of the cluster model were saturated by methyl groups to maintain original hybridization. Double-ξ numerical polarization (DNP) with the PW91 functional set was used in the DFT calculations. The basic principal of the DNP set is that it incorporates p-type polarization into hydrogen atoms and d-type polarization into heavier carbon atoms. The atomic charges calculated from DFT calculations were evaluated by fitting to the electrostatic potential function using the Merz−Kollan (MK) scheme.[35,36]

The prediction of CO_2 and CH_4 uptake inside the nLi_6C_{60}@PAF structures were calculated by the Grand Canonical Monte Carlo (GCMC) routine. GCMC has been used widely for the simulated separation of CO_2/CH_4 mixtures.[17,21,37−40] CO_2 was represented as a three-site rigid molecule, and its intrinsic quadrupole moment was described by a partial charge model. The partial charges on C and O atoms were q_c = 0.576e and q_0 = −0.288e, respectively. The CO_2−CO_2 intermolecular interactions were modeled as a combination of Lennard-Jones (LJ) and Coulombic potentials,

$$U_{ij}(r) = 4\varepsilon_{ij}\left[\left(\frac{\sigma_{ij}}{r_{ij}}\right)^{12} - \left(\frac{\sigma_{ij}}{r_{ij}}\right)^{6}\right] + \frac{q_i q_j}{4\pi\varepsilon_0 r} \quad (1)$$

#tab;where r is the distance between two atoms, σ_{ij} and ε_{ij} are collision diameter and potential well depth, respectively, q_i and q_j are partial charges located at site i and j, respectively, and ε_0 = 8.8542×10^{-12} C/(N/m^2) is the permittivity of a vacuum. The long-range electrostatic interactions were handled via the Ewald summation method. CH_4 was represented by a united-atom model[41] with the LJ potential parameters.[42] Lorentz−Berthelot mixing rules[43] were applied to calculate the interaction between PAFs, lithium, fullerene, CO_2 and CH_4. The force fields adopted were used previously and have been compared with the experimental data, listed in Table 1.[44−46]

Table 1. Lennard-Jones and and Coulombic Parameters[a]

	LJ and Coulombic potential				
species	site	σ (Å)	ε/k_B (K)	q(e)	ref
CO_2	C	2.789	29.66	+0.576	51
	O	3.011	82.96	−0.288	
CH_4	C	3.73	148	0	51
CH_4−C_{60}	C_{CH_4}−C_{60}	3.5805	70.5		52
CO_2−C_{60}	C_{CO_2}−C_{60}	3.11	32.33		45
	O_{CO_2}−C_{60}	3.16	54.6		
CH_4−PAF	C_{CH_4}−C_P^2	3.36	225.44		53
	C_{CH_4}−C_P^3	3.90	80.52	see Supporting Information	
	C_{CH_4}−H_P	2.75	24.16		
CO_2−PAF	C_{CO_2}−C_P^2	3.8	69.44		54
Li-CH_4	Li−CH_4	2.89	59.88		55
Li-CO_2	Li−C_{CO_2}	2.4865	19.32		
	Li−O_{CO_2}	2.5975	32.31		

[a]Here, C_P^3 and C_P^2 represent sp^3 and sp^2 carbon atoms in all PAFs, respectively.

DOI: 10.1021/acs.jpcc.5b01144
J. Phys. Chem. C 2015, 119, 9347−9354

DFT calculations were performed with the Vienna Ab Initio simulation package (VASP)[47] to calculate the CO_2−PAF and CO_2−Li_6C_{60} binding energies. The projector augmented wave (PAW) methods[48] were used to describe the core and valence electrons. The Perdew−Burke−Ernzerhof (PBE)[49] was used to describe the electron exchange and correlations. The DFT-D2 method[50] was applied for the long-term van der Waals dispersion corrections. The Brillouin zone was sampled centered γ centered k-point mesh. The binding energy was calculated according to the formula:

$$E_{\text{binding}} = E_{\text{substrate+gas}} - E_{\text{substrate}} - E_{\text{gas}} \quad (2)$$

GCMC simulations were carried out for the adsorption of single components within the range of frameworks. As a widely used technique to simulate adsorption, GCMC allows the comparison of adsorbate chemical potentials in both adsorbed and bulk phases. In this method, the adsorbent structures were treated as a rigid body. A total of 10^7 trial moves were used for equilibration and another 10^7 moves for the production steps to calculate the average amount of adsorbed gas molecules. To verify the force field, comparisons were made to experimental single component CO_2 isotherms[24] (Figure 2).

IAST has proven an effective method for predicting gas mixtures within a wide variety of porous materials, such as zeolites,[17,56] MOFs,[9,57] and ZIFs.[21,38,58] The method considers the spreading pressure of each gas upon a uniform surface. Perez-Carbajo et al.[59] recently demonstrated that IAST could reasonably describe the mixed adsorption of a five component mixture (CO_2, CH_4, CO, N_2, and H_2) within a range of zeolites (FAU, MFI, MOR, and DDR) up to 100 bar. Here the method was utilized to calculate the selectivity across a range of feed composition ratios.

III. RESULTS AND DISCUSSION

The effect of Li_6C_{60} impregnation upon adsorption up to 2 bar and 298 K is shown in Figure 2a−c for CO_2 and for CH_4 in Figure 3a−c for PAF-302, PAF-303, and PAF-304, respectively. The trends are highlighted with arrows. CO_2 uptake reaches a maximum at a particular amount of Li_6C_{60} whereas the CH_4 uptake continually decreases with impregnation.

The maximum uptake of CO_2 at 2 bar was found to be 15.6 mmol/g in PAF-302 impregnated with one Li_6C_{60} molecule, which is approximately a 100% increase in adsorption capacity compared to that of the bare PAF. The maximum CO_2 uptakes for PAF-303 and PAF-304 were 12 and 11.5 mmol/g with 10 Li_6C_{60} and 27 Li_6C_{60}, respectively, which are approximately a 98% and 47% increases compared to uptakes of bare PAF-303 and PAF-304. Moreover, the maximum numbers of impregnated Li_6C_{60} that can fit within the PAF unit cells are 6, 17, and 40 for PAF-302, PAF-303, and PAF-304, respectively.

There are two reasons for the maximum CO_2 uptake at a particular loading. One reason is that the highest N_2 accessible volumetric surface area (m^2/cm^3) was reached at that particular loading, shown in Figure 4. The second reason is that the interactions between CO_2 and Li_6C_{60} are strong whereas for CH_4 these interactions are negligible, shown in Figure 5. Therefore, the CO_2 uptake increases with the increased surface area whereas CH_4 uptake does not benefit from the increased surface area and rather is inhibited by the loss in pore volume.

The volumetric surface area was found to correlate with the CO_2 uptake (Figure 4). Upon impregnation of Li_6C_{60} in all three PAFs, the surface area and the CO_2 uptake both increase up to a maximum level followed by a decrease with further

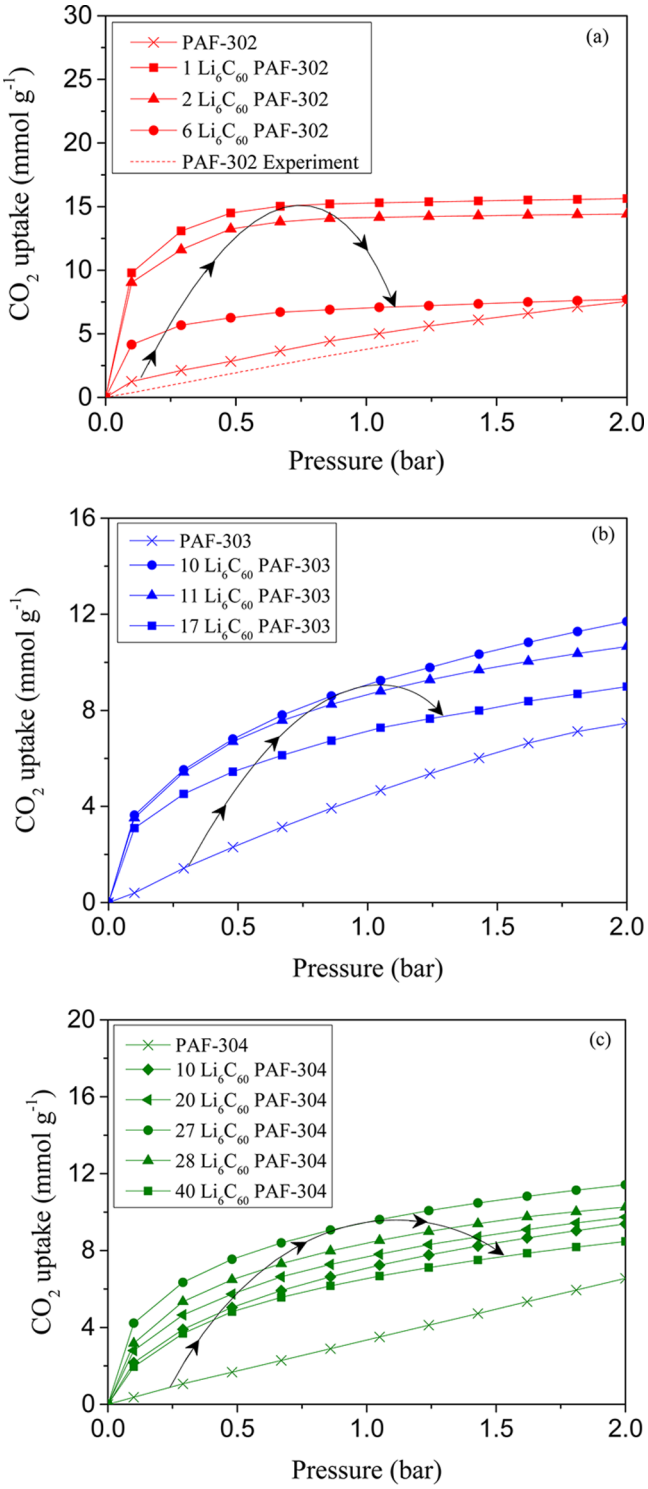

Figure 2. CO_2 uptake at 2 bar and 298 K for Li_6C_{60} impregnated (a) PAF-302, (b) PAF-303, and (c) PAF-304. The red dotted line is the experimental results of CO_2 uptake in bare PAF-302 from Konstas et al.[24] Arrows emphasize the trends with the increasing amount of impregnation.

Li_6C_{60} loading. The maximum volumetric surface areas of 2096, 2140, and 2109 m^2/cm^3 were achieved for PAF-302, PAF-303, and PAF-304, respectively, with corresponding numbers of Li_6C_{60} molecules of 1, 10, and 27. Therefore, the maximum CO_2 uptake is a result of maximizing the volumetric surface area with impregnation. Frost et al.[60] also observed structure−

DOI: 10.1021/acs.jpcc.5b01144
J. Phys. Chem. C 2015, 119, 9347−9354

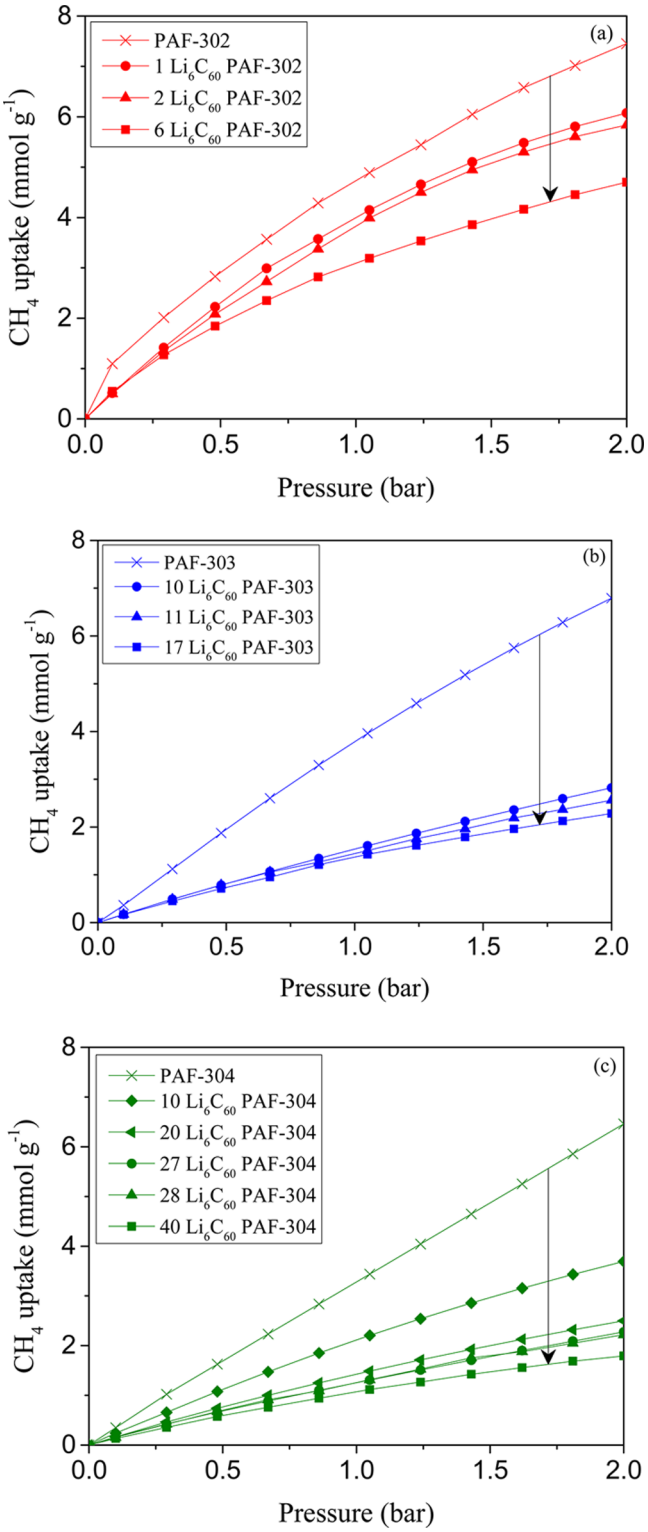

Figure 3. CH_4 uptake at 2 bar and 298 K for Li_6C_{60} impregnated (a) PAF-302, (b) PAF-303, and (c) PAF-304. Arrows emphasize the trends with the increasing amount of impregnation.

property relationships that were pressure-dependent. These trends are confirmed here within the medium to low range of pressures where impregnation and ligand extension allows the control of both the surface area and pore volume.

The isosteric heat of adsorption (q_{st}) for CO_2 and CH_4 is shown in Figure 5a,c, respectively, and is directly related to the

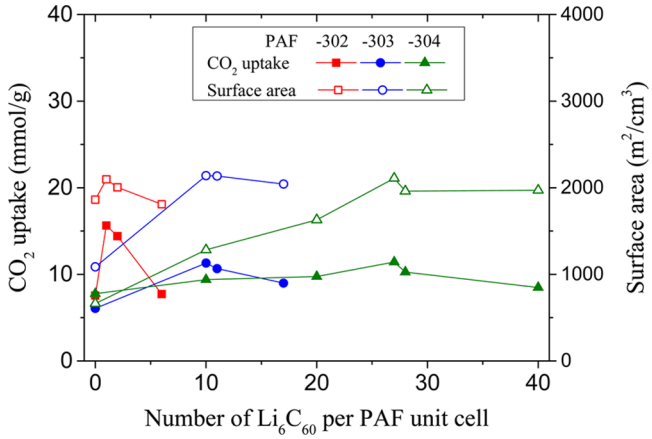

Figure 4. Structure property relationships among CO_2 uptake, Li_6C_{60} loading and volumetric surface area at 2 bar and 298 K. Solid symbols represent CO_2 uptake in PAFs, and open symbols represent the volumetric surface area of corresponding PAFs.

gas−framework interaction strength. The q_{st} in bare PAF-303 and PAF-304 for CO_2 is in the ranges 16−18 and 17−19 kJ/mol, respectively, whereas, for 10 Li_6C_{60} PAF-303 and 27 Li_6C_{60} PAF-304 this value reaches maximum ranges of 39−41 and 41−43 kJ/mol, respectively. These values are in agreement with DFT-based calculations that predict a binding energy of 19 and 45 kJ/mol for CO_2 on PAF and Li_6C_{60}, respectively, Figure 5b. These q_{st} values of CO_2 in impregnated PAFs are much higher than CH_4 q_{st} values, which are 17 and 18 kJ/mol for 10Li_6C_{60} PAF-303 and 27Li_6C_{60} PAF-304, respectively. These high differences in q_{st} values also indicate the promise for high selectivity of CO_2 over CH_4.

The radial distribution function (RDF) between Li_6C_{60} in PAF-304 and the guest molecules is shown in Figure S2 of Supporting Information. A peak in $g(r)$ for CO_2 is observed at r = 4 Å, indicating a high density of CO_2 close to charged Li_6C_{60}, whereas no significant peaks exist for CH_4, indicating bulk-like gas behavior. This confirms that CO_2 interacts strongly with the Li_6C_{60} surface within the PAF, forming an adsorbed layer, whereas CH_4 molecules interact weakly. Considering this, an adsorbed layer that is denser than the bulk gas phase will enhance the overall uptake and will correlate directly with the available surface area. For CH_4, on the contrary, there is only bulk gas phase present, which correlates with the accessible pore volume that continually decreases with impregnation.

The adsorption separation factor is defined by $S_{i/j} = (x_i/x_j)(y_j/y_i)$, where x_i and y_i are the mole fraction of component i in the adsorbed phase and the bulk feed, respectively. For ideal selectivity $y_j/y_i = 1$, and therefore, $S_{i/j} = x_i/x_j$. Here, the ideal gas selectivity for CO_2/CH_4 was plotted against CO_2 uptake in Figure 6a−c and Figure S2 (in Supporting Information) for pressures up to 2 bar. This can be defined as a trade-off plot where a maximum selectivity along with a maximum uptake is desired. The highest selectivities were observed for 27 Li_6C_{60} PAF-304, 10 Li_6C_{60} PAF-303, and 1 Li_6C_{60} PAF-302. Both selectivity and uptake increased up to an optimum number of Li_6C_{60} loading and then decreased with further impregnation.

For industrial application, the mixed selectivity is of interest. Here we predict the mixed selectivity using IAST for different ratios of CO_2:CH_4 (Figure 7 and Figure S3, Supporting Information). The feed composition is assumed to be 20:80. From the IAST predictions we observe a reduced CO_2 uptake and an increased selectivity. This is because the CO_2 will

DOI: 10.1021/acs.jpcc.5b01144
J. Phys. Chem. C 2015, 119, 9347−9354

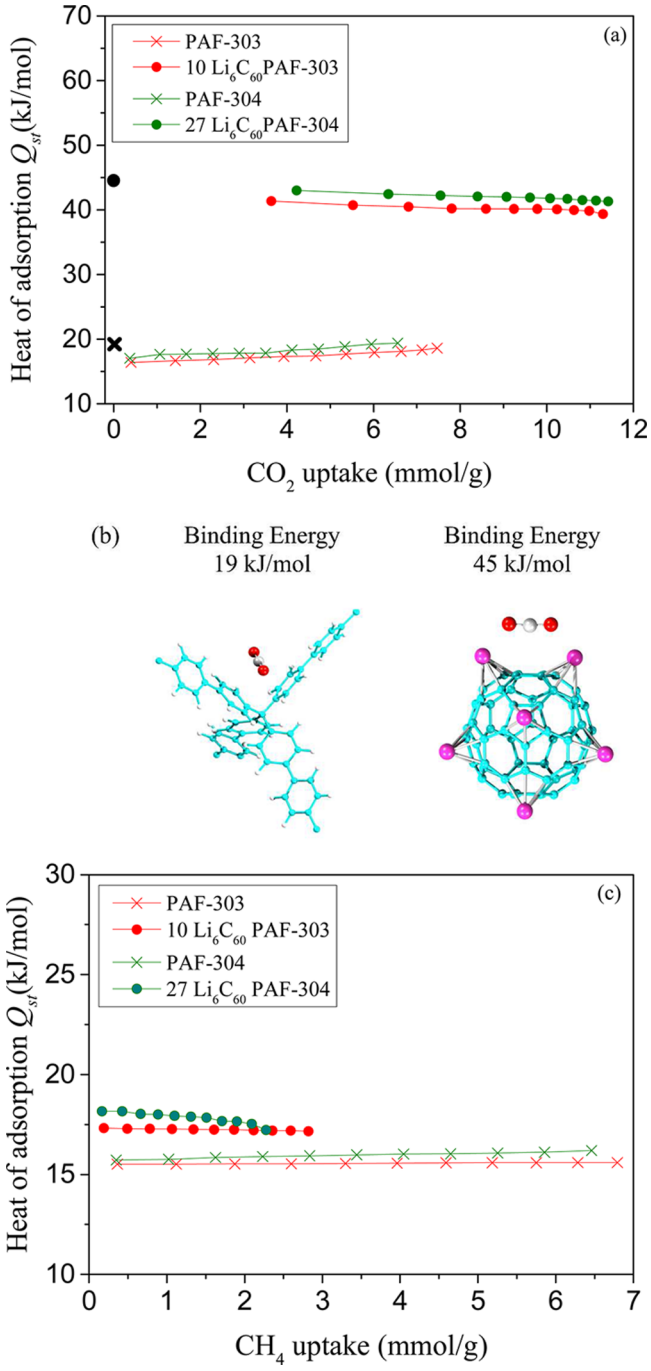

Figure 5. (a) CO_2 isosteric heats of adsorption with DFT-based binding energy values (solid black symbols). (b) Strongest binding sites for CO_2 on PAF and Li_6C_{60} from DFT calculations with binding energies. (c) Isosteric heats of adsorption of CH_4 in bare PAFs and impregnated PAFs.

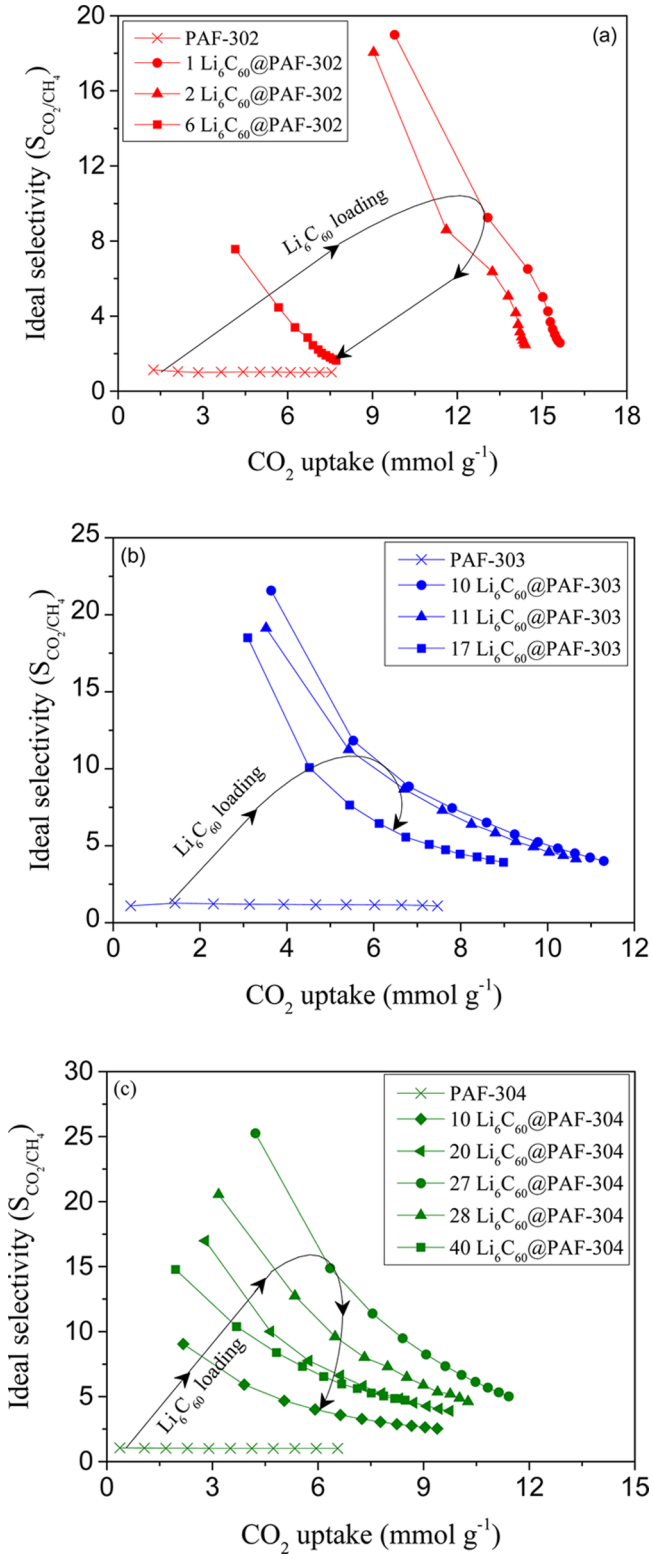

Figure 6. Ideal selectivity CO_2/CH_4 vs CO_2 uptake at 298 K in Li_6C_{60} impregnated (a) PAF-302, (b) PAF-303, and (c) PAF-304. Arrows emphasize the trends with the increasing amount of impregnation.

dominate available adsorption sites over CH_4 but at a loss of capacity. For a higher selectivity, fewer separation stages are required and for higher CO_2 uptake less material is required. For all gas mixture ratios, the selectivity of the impregnated PAFs followed the following order 27 Li_6C_{60} PAF-304 > 10 Li_6C_{60} PAF-303. The IAST mixture adsorption also indicated that Li_6C_{60} impregnation within PAFs enhanced the separation efficiency of an adsorbed based system. The separation of CO_2 from the 20:80 CO_2:CH_4 mixture is 47 and 31 for 27 Li_6C_{60} PAF-304 and 10 Li_6C_{60} PAF-303, respectively, which are larger than other promising adsorbents such as covalent organic frameworks, zeolitic imidazolate frameworks and IRMOF-1.[61,62] The selectivities are also above the zeolite 5A currently used within industry.[63]

DOI: 10.1021/acs.jpcc.5b01144
J. Phys. Chem. C 2015, 119, 9347−9354

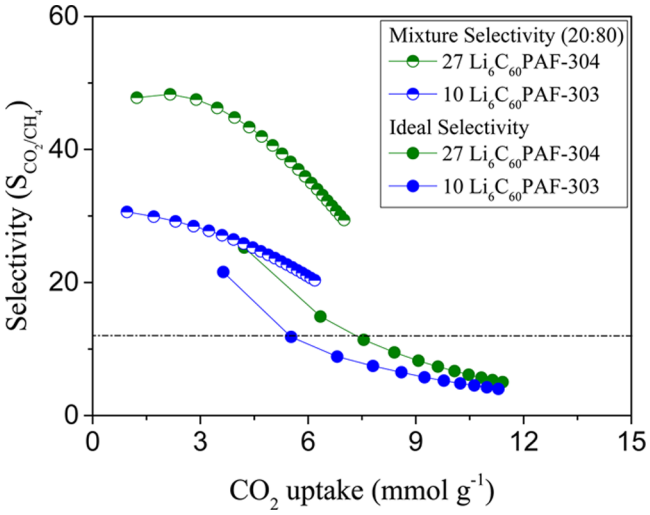

Figure 7. Selectivity vs CO_2 uptake at 298 K in 27 Li_6C_{60} PAF-304 and 10 Li_6C_{60} PAF-303 at various pressures. The dashed line is selectivity value for the most commercially used zeolite 5A.[63]

Finally, comparisons with simulated performances for other materials[64] were made (Figure 8). Here, the ideal selectivity

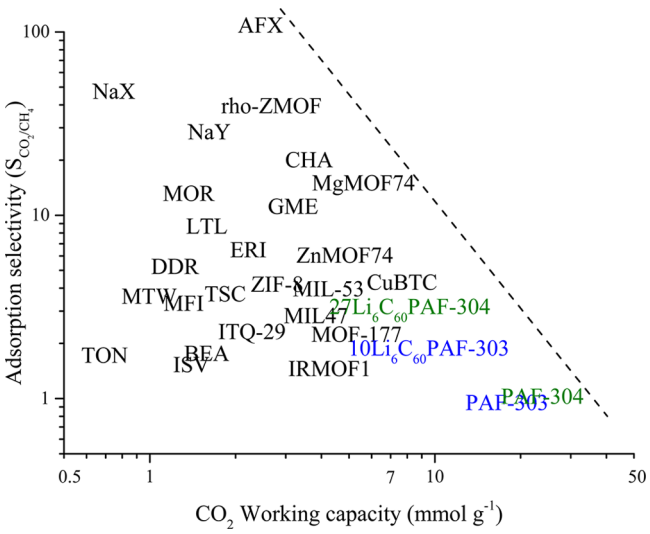

Figure 8. Adsorption selectivities vs working capacity (adsorption cycle between 1 and 1 bar) for CO_2/CH_4 mixtures at 300 K in a variety of MOFs, zeolite, and PAFs structures. Dashed line highlights the upper bound trade-off trend.

and the working capacity (or delta loading) were used. The working capacity is defined as the difference between uptakes at desorption (1 bar) and adsorption (10 bar) pressures. Twenty-seven Li_6C_{60} PAF-304 and 10 Li_6C_{60} PAF-303 showed moderate selectivities with relatively high working capacities compared to those of the other adsorbents. Higher selectivities were found at 2 bar, which means that the separation could be performed at lower pressures, assuming that the materials is completed evacuated of gas. This could possible reduce the energy requirements for separation.

There is an apparent upper bound trend observed for all the adsorbents, as highlighted by a dashed line in Figure 8. For our materials, an increase in selectivity is associated with a loss in working capacity. Within the membrane literature this has been correlated with the size of the gas molecules. This may not be the case for adsorbents.

IV. CONCLUSION

The adsorption of CO_2/CH_4 mixtures has been investigated using molecular simulation for Li_6C_{60} impregnated PAF structures. The simulation isotherms for pure components of CO_2 and CH_4 are in good agreement with the literature.[24] The highest adsorption selectivity for CO_2 over CH_4 is predicted as 47−48 for 27 Li_6C_{60} PAF-304 and 30−31 for 10 Li_6C_{60} PAF-303. The highest volumetric surface area correlated with the highest CO_2/CH_4 selectivity and the highest CO_2 uptake at the optimal Li_6C_{60} loading. The results show that the available surface area within 27 Li_6C_{60} PAF-304 and 10 Li_6C_{60} PAF-303 offer stronger adsorption sites for CO_2 than for CH_4. The high CO_2 adsorption selectivity at 2 bar suggests that Li_6C_{60}@ PAF could be successfully used for natural gas (CH_4) purification.

In comparison with other adsorbents, the impregnated PAFs showed moderate selectivities with relatively high working capacities at standard operating conditions cycling between 1 and 10 bar. There is an apparent upper bound trade-off between selectivity and capacity that the impregnated PAFs cannot overcome. Overall, the impregnated PAFs have tunable surface areas and porosity to customize separation requirements.

■ ASSOCIATED CONTENT

Supporting Information

Table S1 shows the composition of natural gas reservoirs across the world. Figure S1 shows the charge assignment within the frameworks for (a) PAF-302 (four types of carbon and one type of hydrogen atom), (b) PAF-303 (eight types of carbon and two types of hydrogen atom), (c) PAF-304 (eight types of carbon and two types of hydrogen atom), and (d) Li6C60 (three types of carbon and one type of lithium atom). Figure S2 shows the radial distribution function $g(r)$ between the Li_6C_{60} and the center of mass for CO_2 and CH_4 molecules. Figure S3 shows the ideal selectivity of CO_2/CH_4 at 298 K and 2 bar. Figure S4 shows the selectivity vs CO_2 uptake at 298 K in (a) 27 Li_6C_{60} PAF-304 and (b) 10 Li_6C_{60} PAF-303 for different ratios of CO_2:CH_4. This material is available free of charge via the Internet at http://pubs.acs.org.

■ AUTHOR INFORMATION

Corresponding Author

*A. W. Thornton. Tel: +61418438423. E-mail: aaron.thornton@csiro.au.

Notes

The authors declare no competing financial interest.

■ ACKNOWLEDGMENTS

A.A. acknowledges the top-up scholarship provided by the CSIRO Computational and Simulation Sciences Transformational Capability Platform and the full scholarship provided by Swinburne University. The authors acknowledge the computational facilities and services provided through the CSIRO Advanced Scientific Computing, Monash Sun Grid, and the National Computing Infrastructure facilities. M.R.H. acknowledges the ARC for support (FT130100345).

DOI: 10.1021/acs.jpcc.5b01144
J. Phys. Chem. C 2015, 119, 9347−9354

REFERENCES

(1) Cavenati, S.; Grande, C. A.; Rodrigues, A. E. Adsorption Equilibrium of Methane, Carbon Dioxide, and Nitrogen on Zeolite 13x at High Pressures. *J. Chem. Eng. Data* **2004**, *49*, 1095−1101.

(2) Shimekit, B.; Mukhtar, H. *Natural Gas Purification Technologies - Major Advances for CO_2 Separation and Future Directions*; INTECH Open Access Publisher: Croatia, Europe, 2012.

(3) Yang, R. T. *Gas Separation by Adsorption Processes*; Imperial College Press.: London, 1997.

(4) Li, Y.; Chung, T. S.; Kulprathipanja, S. Novel Ag+-Zeolite/Polymer Mixed Matrix Membranes with a High CO_2/CH_4 Selectivity. *AlChE J.* **2007**, *53*, 610−616.

(5) Shimekit, B.; Mukhtar, H. *Natural Gas Purification Technologies - Major Advances for Co_2 Separation and Future Directions*; INTECH Open Access Publisher: Croatia, Europe, 2012.

(6) Dortmundt, D.; Doshi, K. *Recent Developments in CO_2 Removal Membrane Technology*; UOP LLC: Des Plaines, IL, 1999.

(7) Krooss, B.; Van Bergen, F.; Gensterblum, Y.; Siemons, N.; Pagnier, H.; David, P. High-Pressure Methane and Carbon Dioxide Adsorption on Dry and Moisture-Equilibrated Pennsylvanian Coals. *Int. J. Coal. Geol.* **2002**, *51*, 69−92.

(8) White, C. M.; Smith, D. H.; Jones, K. L.; Goodman, A. L.; Jikich, S. A.; LaCount, R. B.; DuBose, S. B.; Ozdemir, E.; Morsi, B. I.; Schroeder, K. T. Sequestration of Carbon Dioxide in Coal with Enhanced Coalbed Methane Recovery a Review. *Energy Fuel* **2005**, *19*, 659−724.

(9) Liu, B.; Smit, B. Comparative Molecular Simulation Study of Co_2/N_2 and Ch_4/N_2 Separation in Zeolites and Metal−Organic Frameworks. *Langmuir* **2009**, *25*, 5918−5926.

(10) Ebenezer, S. A.; Gudmundsson, J. Tracer Behaviour in Pipelines with Deposits and Analysis of Natural Gas Pressure Functions. Diploma, Norwegian University of Science and Technology, Norway, July 2006.

(11) Kohl, A. L.; Nielsen, R. *Gas Purification*; Gulf Professional Publishing: Houston, TX, 1997.

(12) Mersmann, A.; Kind, M.; Stichlmair, J. *Thermal Separation Technology*; Springer: Verlag Berlin Heidelberg, 2011; Vol. *646*.

(13) Kerry, F. G. *Industrial Gas Handbook: Gas Separation and Purification*; CRC Press: Boca Raton, FL, 2010.

(14) Shekhawat, D.; Luebke, D. R.; Pennline, H. W. *A Review of Carbon Dioxide Selective Membranes*; National Energy Technology Lab: Pittsburgh, PA, 2003.

(15) Porter, M. C. *Handbook of Industrial Membrane Technology*; Noyes Publications: Park Ridge, NJ, 1989; Vol. *62*, p 765.

(16) Li, J.-R.; Kuppler, R. J.; Zhou, H.-C. Selective Gas Adsorption and Separation in Metal−Organic Frameworks. *Chem. Soc. Rev.* **2009**, *38*, 1477−1504.

(17) Babarao, R.; Hu, Z.; Jiang, J.; Chempath, S.; Sandler, S. I. Storage and Separation of CO_2 and CH_4 in Silicalite, C168 Schwarzite, and IRMOF-1: A Comparative Study from Monte Carlo Simulation. *Langmuir* **2006**, *23*, 659−666.

(18) Yang, Z.; Peng, X.; Cao, D. Carbon Dioxide Capture by PAFs and an Efficient Strategy to Fast Screen Porous Materials for Gas Separation. *J. Phys. Chem. C* **2013**, *117*, 8353−8364.

(19) Li, Y.; Yi, H.; Tang, X.; Li, F.; Yuan, Q. Adsorption Separation of CO_2/CH_4 Gas Mixture on the Commercial Zeolites at Atmospheric Pressure. *Chem. Eng. J.* **2013**, *229*, 50−56.

(20) Babarao, R.; Jiang, J.; Sandler, S. I. Molecular Simulations for Adsorptive Separation of CO_2/CH_4 Mixture in Metal-Exposed, Catenated, and Charged Metal−Organic Frameworks. *Langmuir* **2008**, *25*, 5239−5247.

(21) Liu, B.; Smit, B. Molecular Simulation Studies of Separation of CO_2/N_2, CO_2/CH_4, and CH_4/N_2 by ZIFs. *J. Phys. Chem. C* **2010**, *114*, 8515−8522.

(22) Ebner, A. D.; Ritter, J. A. State-of-the-Art Adsorption and Membrane Separation Processes for Carbon Dioxide Production from Carbon Dioxide Emitting Industries. *Sep. Sci. Technol.* **2009**, *44*, 1273−1421.

(23) Ben, T.; Pei, C.; Zhang, D.; Xu, J.; Deng, F.; Jing, X.; Qiu, S. Gas Storage in Porous Aromatic Frameworks (PAFs). *Energy Environ. Sci.* **2011**, *4*, 3991−3999.

(24) Konstas, K.; Taylor, J. W.; Thornton, A. W.; Doherty, C. M.; Lim, W. X.; Bastow, T. J.; Kennedy, D. F.; Wood, C. D.; Cox, B. J.; Hill, J. M. Lithiated Porous Aromatic Frameworks with Exceptional Gas Storage Capacity. *Angew. Chem., Int. Ed.* **2012**, *124*, 6743−6746.

(25) He, L.-N.; Rogers, R. D.; Su, D.; Tundo, P.; Zhang, Z. C. *Porous Materials for Carbon Dioxide Capture*; Springer Verlag: Berlin, Heidelberg, 2014; pp 1−253.

(26) Yuan, D.; Lu, W.; Zhao, D.; Zhou, H. C. Highly Stable Porous Polymer Networks with Exceptionally High Gas-Uptake Capacities. *Adv. Mater.* **2011**, *23*, 3723−3725.

(27) Ahmed, A.; Thornton, A. W.; Konstas, K.; Kannam, S. K.; Babarao, R.; Todd, B. D.; Hill, A. J.; Hill, M. R. Strategies toward Enhanced Low-Pressure Volumetric Hydrogen Storage in Nanoporous Cryoadsorbents. *Langmuir* **2013**, *29*, 15689−15697.

(28) Peng, X.; Cao, D.; Wang, W. Computational Study on Purification of CO_2 from Natural Gas by C_{60} Intercalated Graphite. *Ind. Eng. Chem. Res.* **2010**, *49*, 8787−8796.

(29) Myers, A.; Prausnitz, J. M. Thermodynamics of Mixed-Gas Adsorption. *AlChE J.* **1965**, *11*, 121−127.

(30) Alawisi, H.; Li, B.; He, Y.; Arman, H. D.; Asiri, A. M.; Wang, H.; Chen, B.; Microporous, A. Metal−Organic Framework Constructed from a New Tetracarboxylic Acid for Selective Gas Separation. *Cryst. Growth Des.* **2014**, *14*, 2522−2526.

(31) Lan, J.; Cao, D.; Wang, W.; Ben, T.; Zhu, G. High-Capacity Hydrogen Storage in Porous Aromatic Frameworks with Diamond-Like Structure. *J. Phys. Chem. Lett.* **2010**, *1*, 978−981.

(32) Farha, O. K.; Eryazici, I.; Jeong, N. C.; Hauser, B. G.; Wilmer, C. E.; Sarjeant, A. A.; Snurr, R. Q.; Nguyen, S. T.; Yazaydın, A. Ö.; Hupp, J. T. Metal−Organic Framework Materials with Ultrahigh Surface Areas: Is the Sky the Limit? *J. Am. Chem. Soc.* **2012**, *134*, 15016−15021.

(33) Babarao, R.; Dai, S.; Jiang, D.-e. Functionalizing Porous Aromatic Frameworks with Polar Organic Groups for High-Capacity and Selective CO_2 Separation: A Molecular Simulation Study. *Langmuir* **2011**, *27*, 3451−3460.

(34) Krishna, R. Diffusion of Binary Mixtures across Zeolite Membranes: Entropy Effects on Permeation Selectivity. *Ind. Eng. Chem. Res.* **2001**, *28*, 337−346.

(35) Besler, B. H.; Merz, K. M.; Kollman, P. A. Atomic Charges Derived from Semiempirical Methods. *J. Comput. Chem.* **1990**, *11*, 431−439.

(36) Chirlian, L. E.; Francl, M. M. Atomic Charges Derived from Electrostatic Potentials: A Detailed Study. *J. Comput. Chem.* **1987**, *8*, 894−905.

(37) Babarao, R.; Jiang, J. Diffusion and Separation of CO_2 and CH_4 in Silicalite, C168 Schwarzite, and IRMOF-1: A Comparative Study from Molecular Dynamics Simulation. *Langmuir* **2008**, *24*, 5474−5484.

(38) Liu, J.; Keskin, S.; Sholl, D. S.; Johnson, J. K. Molecular Simulations and Theoretical Predictions for Adsorption and Diffusion of CH_4/H_2 and CO_2/CH_4 Mixtures in ZIFs. *J. Phys. Chem. C* **2011**, *115*, 12560−12566.

(39) Li, W.; Shi, H.; Zhang, J. From Molecules to Materials: Computational Design of N-Containing Porous Aromatic Frameworks for CO_2 Capture. *ChemPhysChem* **2014**, *15*, 1772−1778.

(40) Kong, L.; Zou, R.; Bi, W.; Zhong, R.; Mu, W.; Liu, J.; Han, R. P.; Zou, R. Selective Adsorption of CO_2/CH_4, CO_2/N_2 within a Charged Metal-Organic Framework. *J. Mater. Chem. A* **2014**, *2*, 17771−17778.

(41) Ryckaert, J.-P.; Bellemans, A. Molecular Dynamics of Liquid Alkanes. *Faraday Discuss. Chem. Soc.* **1978**, *66*, 95−106.

(42) Eddaoudi, M.; Kim, J.; Rosi, N.; Vodak, D.; Wachter, J.; O'Keeffe, M.; Yaghi, O. M. Systematic Design of Pore Size and Functionality in Isoreticular MOFs and Their Application in Methane Storage. *Science* **2002**, *295*, 469−472.

DOI: 10.1021/acs.jpcc.5b01144
J. Phys. Chem. C 2015, 119, 9347−9354

(43) Kwak, T. Y.; Mansoori, G. A. Van Der Waals Mixing Rules for Cubic Equations of State, Applications for Supercritical Fluid Extraction Modelling. *Chem. Eng. Sci.* **1986**, *41*, 1303−1309.
(44) Mendoza-Cortés, J. L.; Han, S. S.; Furukawa, H.; Yaghi, O. M.; Goddard, W. A., III. Adsorption Mechanism and Uptake of Methane in Covalent Organic Frameworks: Theory and Experiment. *J. Phys. Chem. A* **2010**, *114*, 10824−10833.
(45) Martínez-Alonso, A.; Tascón, J. M. D.; Bottani, E. J. Physical Adsorption of Ar and CO_2 on C_{60} Fullerene. *J. Phys. Chem. B* **2000**, *105*, 135−139.
(46) Cao, D.; Lan, J.; Wang, W.; Smit, B. Lithium-Doped 3d Covalent Organic Frameworks: High-Capacity Hydrogen Storage Materials. *Angew. Chem., Int. Ed.* **2009**, *121*, 4824−4827.
(47) Kresse, G.; Furthmüller, J. Efficiency of Ab-Initio Total Energy Calculations for Metals and Semiconductors Using a Plane-Wave Basis Set. *Comput. Mater. Sci.* **1996**, *6*, 15−50.
(48) Blöchl, P. E. Projector Augmented-Wave Method. *Phys. Rev. B* **1994**, *50*, 17953.
(49) Perdew, J. P.; Burke, K.; Ernzerhof, M. Generalized Gradient Approximation Made Simple. *Phys. Rev. Lett.* **1996**, *77*, 3865.
(50) Grimme, S. Semiempirical GGA-Type Density Functional Constructed with a Long-Range Dispersion Correction. *J. Comput. Chem.* **2006**, *27*, 1787−1799.
(51) Chen, Y. F.; Lee, J. Y.; Babarao, R.; Li, J.; Jiang, J. W. A Highly Hydrophobic Metal−Organic Framework $Zn(BDC)(TED)_{0.5}$ for Adsorption and Separation of CH_3OH/H_2O and CO_2/CH_4: An Integrated Experimental and Simulation Study. *J. Phys. Chem. C* **2010**, *114*, 6602−6609.
(52) Whitener, K. E. Theoretical Studies of CH_4 inside an Open-Cage Fullerene: Translation−Rotation Coupling and Thermodynamic Effects. *J. Phys. Chem. A* **2010**, *114*, 12075−12082.
(53) Cossi, M.; Gatti, G.; Canti, L.; Tei, L.; Errahali, M.; Marchese, L. Theoretical Prediction of High Pressure Methane Adsorption in Porous Aromatic Frameworks (PAFs). *Langmuir* **2012**, *28*, 14405−14414.
(54) Fraccarollo, A.; Canti, L.; Marchese, L.; Cossi, M. Monte Carlo Modeling of Carbon Dioxide Adsorption in Porous Aromatic Frameworks. *Langmuir* **2014**, *30*, 4147−4156.
(55) Lan, J.; Cao, D.; Wang, W. High Uptakes of Methane in Li-Doped 3d Covalent Organic Frameworks. *Langmuir* **2009**, *26*, 220−226.
(56) Goj, A.; Sholl, D. S.; Akten, E. D.; Kohen, D. Atomistic Simulations of CO_2 and N_2 Adsorption in Silica Zeolites: The Impact of Pore Size and Shape. *J. Phys. Chem. B* **2002**, *106*, 8367−8375.
(57) Bae, Y.-S.; Farha, O. K.; Spokoyny, A. M.; Mirkin, C. A.; Hupp, J. T.; Snurr, R. Q. Carborane-Based Metal-Organic Frameworks as Highly Selective Sorbents for CO_2 over Methane. *Chem. Commun.* **2008**, *38*, 4135−4137.
(58) Thornton, A. W.; Dubbeldam, D.; Liu, M. S.; Ladewig, B. P.; Hill, A. J.; Hill, M. R. Feasibility of Zeolitic Imidazolate Framework Membranes for Clean Energy Applications. *Energy Environ. Sci.* **2012**, *5*, 7637−7646.
(59) Perez-Carbajo, J.; Gomez-Alvarez, P.; Bueno-Perez, R.; Merkling, P. J.; Calero, S. Optimisation of the Fischer−Tropsch Process Using Zeolites for Tail Gas Separation. *Phys. Chem. Chem. Phys.* **2014**, *16*, 5678−5688.
(60) Frost, H.; Duren, T.; Snurr, R. Q. Effects of Surface Area, Free Volume, and Heat of Adsorption on Hydrogen Uptake in Metal-Organic Frameworks. *J. Phys. Chem. B* **2006**, *110*, 9565−9570.
(61) Yang, Q.; Zhong, C. Molecular Simulation of Carbon Dioxide/Methane/Hydrogen Mixture Adsorption in Metal-Organic Frameworks. *J. Phys. Chem. B* **2006**, *110*, 17776−17783.
(62) Liu, Y.; Liu, D.; Yang, Q.; Zhong, C.; Mi, J. Comparative Study of Separation Performance of COFs and MOFs for $CH_4/CO_2/H_2$ Mixtures. *Ind. Eng. Chem. Res.* **2010**, *49*, 2902−2906.
(63) Wu, X.; Niknam Shahrak, M.; Yuan, B.; Deng, S. Synthesis and Characterization of Zeolitic Imidazolate Framework ZIF-7 for CO_2 and CH_4 Separation. *Microporous Mesoporous Mater.* **2014**, *190*, 189−196.
(64) Krishna, R.; van Baten, J. M. In Silico Screening of Metal−Organic Frameworks in Separation Applications. *Phys. Chem. Chem. Phys.* **2011**, *13*, 10593−10616.

DOI: 10.1021/acs.jpcc.5b01144
J. Phys. Chem. C 2015, 119, 9347−9354